Numerical Investigation of Internal Wave-Vortex Interactions

Tyler D. Blackhurst
Department of Mechanical Engineering
Brigham Young University, Provo, UT

Internal gravity waves are inherent in the atmosphere and ocean as a result of the stable stratification of these mediums. Internal waves may be generated in many ways, including by flow over topography, convective storms, or turbulent mixing. As they propagate through their medium, internal waves of various scales (tens of meters to tens of kilometers) interact with other fluid flow phenomena found throughout geophysical fluid flows. The interaction of small-scale internal waves with a vortex dipole is of particular interest due to the rotation of the earth resulting in constant vortex generation. The speed and direction with which internal waves approach a vortex dipole can significantly affect the wave-vortex interaction, determining if the energy of the internal waves will be absorbed, refracted, or unaffected by the dipole. The interaction presented involves waves propagating in the same direction as the translation of the dipole. This co-propagating interaction yields a spreading of wave energy, termed defocusing, observed as rays interact with the dipole and then diverge in the spanwise direction. Waves can approach critical levels, where the wave energy is absorbed by the dipole or the waves are overturned and possibly break. As wave breaking cannot be simulated with this linear model, an analysis of changes in wave steepness aids in estimating the onset of breaking. The numerical results support the experimental study of Godoy-Diana, Chomaz and Donnadieu (2006).

Introduction

A stably-stratified fluid is one in which the density increases continuously with depth, such as the ocean or the atmosphere. Perturbations of a stably-stratified fluid, such as tidal flow over topography, move fluid particles of one depth and neutrally-buoyant state to a depth in which they are surrounded by fluid particles of a different density. The surrounding fluid particles push the displaced particles back in the direction of their neutrally-buoyant state. When there is enough momentum to displace the fluid particles in the other direction, oscillations occur until the fluid particles reach a stable location with respect to their density. The stratification strength of the fluid is defined by the Brunt-Väisälä frequency, the natural frequency of the fluid, which involves the change in density over height within the fluid. Oscillations less than this frequency create internal waves which play an integral role in oceanic and atmospheric dynamics, affecting climates and weather patterns, maintaining environmental energy budgets (*i.e.*, mass, momentum and heat), and are a source of turbulence and mixing.

Since early last century scientists and researchers have observed and studied internal wave propagation and evolution in the ocean and atmosphere. Today researchers can numerically simulate internal wave propagation and wave interactions with other fluid phenomena, studying them from every point in space and time, and compare the results with what is known from observation and experimentation. However, reconciling theoretical predictions with experimental data is sometimes problematic since, during wave propagation and interactions, the transport of energy may be at such small scales that observations lack sufficient resolution and the onset of turbulence invalidates two-dimensional linear theories. With three-dimensional simulation capabilities, we can more completely study the generation, propagation and evolution of internal waves and apply more accurate theories and approximations. Such capabilities will also increase knowledge of internal wave interactions and the mechanics of wave breaking.

Internal waves interact with a myriad of flow phenomena, including other internal waves of similar and different scales. Javam, Imberger and Armfield (2000) numerically researched interactions of internal waves of similar scales and found these interactions were nonlinear and involved wave breaking. Broutman and Young (1986) used ray theory (to be described later) to numerically track the changes of small-scale internal waves (on the order of tens of meters) interacting with a large-scale internal wave background (on the order of kilometers and greater). They confirmed theoretical predictions for conditions of internal waves prior to and following the interactions. Winters and D'Asaro (1989) used a two-dimensional model to numerically simulate the propagation of internal waves into a slowly-varying mean shear background. Nonlinearity and three-dimensionality overcome the simulated waves when the internal waves become unstable and turbulence begins, breaking down the internal waves. Later, three-dimensional considerations were discussed by Winters and D'Asaro (1994). Convective instabilities yielded counter-rotating vortices, the effects of which were magnified by wave shear. The combination of convection and shear in these interactions obligate three-dimensional analysis. This obligation is a representative result of all the studies cited thus far and is essential to the continuing discussion.

Vortices are a common occurrence in large, geophysical flows as a result of shear and turbulence in a rotating fluid. Moulin and Flór (2006) numerically demonstrated a three-

dimensional interaction between a large-scale internal wave and a Rankine-type vortex. By varying the initial locations of the internal waves, the authors demonstrated that each wave-vortex interaction resulted in a different scenario with different effects on the internal waves. In some cases, the waves reflected; in others, they were absorbed into the rotating flow; still other combinations produced breaking waves. Despite the wealth of information gained from these simulations, questions remain about what happens to the energy of internal waves during the onset of turbulence and other three-dimensional characteristics during wave-vortex interactions. While we know the waves may break, it is unclear what mechanisms are responsible for their evolution to breaking and how and why turbulence begins.

Godoy-Diana, Chomaz and Donnadieu (2006) discussed the experimental interaction of internal waves with a Lamb-Chaplygin pancake vortex dipole. A vortex dipole involves two side-by-side, counter-rotating vortices; the Lamb-Chaplygin vortex dipole is an exact solution of the Euler equations (Billant, Brancher and Chomaz (1999)). Two experimental cases of wave-vortex interactions were conducted. The first is of internal waves generated by oscillating a cylinder along the width of the domain and then propagating in the same horizontal direction as the translation of the vortex dipole. In this co-propagating case, the wave beam was seen bending to the horizontal and possibly being absorbed by the dipole. The second case is of internal waves propagating opposite to the direction of horizontal translation of the dipole. This counter-propagating case resulted in the beam of internal waves steepening to the vertical and possibly reflecting. In the two-dimensional images taken at the center of these interactions, *i.e.*, wave interactions with the dipole's jet, areas are seen of concentrated wave energy. These are resultant of the internal waves generated by the cylinder but off-center and interacting with regions of the dipole other than its jet. Termed defocusing in the co-propagating case and focusing in the counter-propagating, these results suggest three-dimensional effects are essential in internal wave propagation. A numerical analysis of this experiment illuminates the involved three-dimensional mechanisms, showing what happens to the internal wave properties and energy during the interactions and what may contribute to nonlinear aftereffects (*e.g.*, wave breaking).

This paper details the work and results of numerically modeling a set of small-scale internal waves interacting in three dimensions with a vortex dipole of constant rotation and translation. The next section discusses the experimental setup of Godoy-Diana, *et al.* (2006) and the corresponding numerical setup for the current study, including the mathematical theory. The following section presents the results of the co-propagating interaction simulations, including comparisons to the experiment of Godoy-Diana, *et al.* (2006). The final section discusses the practical impact of the results of the study, further research to be done on this project, and ideas for future research.

Methods

During internal wave interactions, the wave properties may change, particularly the wavenumbers and the relative frequency (frequency of waves propagating in a quiescent medium). If the relative frequency of the internal waves approaches zero in a non-rotating system (the frequency of rotation otherwise, *e.g.*, the Coriolis frequency), a critical level is approached where the energy of the internal waves may be absorbed by the dipole or the waves may overturn and break. If the relative frequency approaches the value of the fluid's buoyancy frequency, a turning point reflects the internal waves. Theoretically, wave energy cannot pass either extremity, for the relative frequency cannot be less than zero nor greater than the buoyancy frequency and maintain the presence of internal waves.

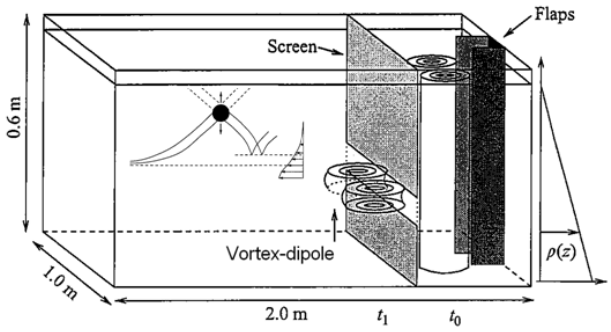

Figure 1a: Saltwater stratified water experimental tank (Godoy-Diana, et al. (2006)). The dipole is created by flaps at one end of the tank and approaches a screen which allows a slice of the dipole to pass into the interaction area with the cylinder generating the internal waves.

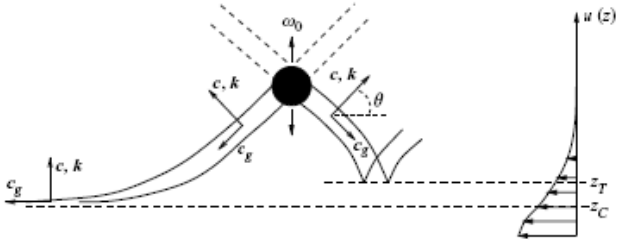

Figure 1b: Close-up view of oscillating cylinder generating internal waves relative to the vortex velocity profile (Godoy-Diana, *et al.* (2006)). The co-propagating case shows the internal waves being absorbed by the vortex. The counter-propagating case shows the internal waves reflecting away from the vortex.

The experimental internal wave-vortex interaction of Godoy-Diana, *et al.* (2006) was completed in a tank of salt-stratified water of constant stratification, as shown in Figure 1a. After the dipole was generated, it approached a screen which allowed only a thin slice of the dipole to pass to the area of interaction. Beams of internal waves were generated above the interaction region by oscillating cylinders at a frequency less than the natural buoyancy frequency of the fluid. Figure 1b shows a close-up representation of the co- and counter-propagating interactions described earlier. The co-propagating wave beam is seen being absorbed into the vortex dipole at a critical level z_C, and the counter-

propagating wave beam is reflected vertically away from the dipole at a turning point z_T.

The numerical code for the current study was written in Matlab. Ray theory governs the numerical simulation. Ray theory, often called ray tracing, traces the directions (rays) of wave propagation before, during, and after the wave-vortex interaction. Ray theory is linear, even in three dimensions, so the basic propagation of the waves, and the effects of interaction, can be simply modeled and the results are easily compared to experimental results and observational data. Ray theory is also quick in its application, providing a method of research much faster and less expensive than experimentation and observation. However, application of linear theories results in inaccurate predictions of nonlinear behavior. Additional calculations involving wave amplitudes and energy are required to estimate through ray theory the onset of nonlinearities.

Ray theory is a method of solving the Navier-Stokes equations, the governing equations of fluid flow. To simplify the Navier-Stokes equations for this case, the propagation of the vortex is assumed slowly varying while the only side-effects of the interaction are changes to the characteristics and propagation of the small-scale internal waves. This is the linear, inviscid Wentzel-Kramer-Brillouin-Jeffreys (WKBJ) approximation. It allows the dispersion relation to be valid locally. While it is not representative of all wave-vortex interactions, this assumption is realistic when waves are interacting with large-scale geophysical flows and is the foundation of ray theory. Another simplification is the Boussinesq approximation, which states that changes in density are negligible except in terms where the acceleration due to gravity is a multiplier. The solution to the Navier-Stokes equations is then a form of the wave equation.

The full ray theory equations are now presented for internal waves interacting with a mean background flow of velocity $\boldsymbol{v}= (v_1, v2, v3)$. The Doppler relation defines the relation between the total frequency Ω of the internal waves in a stationary frame of reference and the relative frequency ω_r of the internal waves in the frame of reference of the moving fluid (*i.e.*, the background velocity),

$$\omega_r = \Omega - v_j k_j \tag{1}$$

where v_j is the component of the background velocity and k_j is the component of the small-scale wavenumber vector $\boldsymbol{k}= (k_1, k_2, k_3)$. The dispersion relation defines ω_r as a function of wavenumber, the buoyancy frequency N, and the Coriolis frequency f,

$$\omega_r^2 = \frac{N^2(k_1^2 + k_2^2) + f^2 k_3{}^2}{k_1^2 + k_2^2 + k_3^2} \tag{2}$$

If the system containing the interaction is non-rotating, f is neglected; it is so in this work.

The velocities of the internal waves are defined by the sum of the mean velocity of the background and the group velocity of the internal waves,

$$\frac{dx_i}{dt} = v_i + \frac{\partial \omega_r}{\partial k_i} \tag{3}$$

for which $\boldsymbol{x}=(x_1, x_2, x_3)$ defines the space of the domain.

The law governing refraction is given by

$$\frac{dk_i}{dt} = -k_j \frac{\partial v_j}{\partial x_i} - \frac{\partial \omega_r}{\partial x_i} \tag{4}$$

To define the change of the relative frequency with respect to time,

$$\frac{d\omega_r}{dt} = \frac{\partial \omega_r}{\partial k_i}\frac{dk_i}{dt} + \frac{\partial \omega_r}{\partial x_i}\frac{dx_i}{dt} \tag{5}$$

The foregoing equations identify how the properties of the internal waves change during an interaction. From these changes, the energy transfer of the waves within the interaction can be determined. This then allows for calculation of wave steepness, from which overturning and breaking may be estimated.

Ray theory energetics begins with wave action A, defined as the product of wave action density A' and volume V held by the waves, a conserved quantity; that is,

$$A = A'V = A'_0 V_0 \tag{6}$$

where the subscript 0 denotes an initial value. Wave action density is not necessarily known, but the volumes can be calculated by following Hayes (1970), so it is easier to rearrange (6) and use

$$\frac{A'}{A'_0} = \frac{1}{V/V_0} \tag{7}$$

The total energy E is defined through the integral

$$E = \int E' dV = \int A' \omega_r dV \tag{8}$$

where E' is energy density. The integrand on the right-hand side is not a function of volume, so total energy is equal to the product of wave action and relative frequency. Because total energy and wave action are not necessarily known, it is easier to consider an energy ratio

$$\frac{E}{E_0} = \frac{A}{A_0}\frac{\omega_r}{\omega_{r0}} \tag{9}$$

Because wave action is conserved, this energy ratio simplifies to the ratio of relative frequency to initial relative frequency only.

Finally, wave steepness η is given by applying (7) and (9)

$$\frac{d\eta}{dz} = k_1 \left| \frac{A'}{A'_0}\frac{E_0}{E} \right|^{1/2} \tag{10}$$

The equations governing the Lamb-Chaplygin vortex dipole are given by Billant, *et al.* (1999). Three non-dimensional control parameters defined the dipole of the interaction: the Reynolds number $Re=UL_h/\nu$; the horizontal

Froude number $Fr_h=U/NL_h$; and the aspect ratio $\alpha=L_v/L_h$; where ν is the kinematic viscosity of salt water and

$$L_h = \sqrt{\frac{\mathrm{Re}\,\nu}{Fr_h N}}$$
$$L_v = \alpha L_h \qquad (11)$$
$$U = \frac{\mathrm{Re}\,\nu}{L_h}$$

are the horizontal length scale (dipole radius), the vertical length scale (dipole thickness in the interaction region) and the dipole translation speed, respectively. Using values from Godoy-Diana, *et al.* (2006) (Re=182, Fr_h=0.18, α=1.27) and a common value for buoyancy frequency (N=0.447 s^{-1}), the dipole properties of (11) were determined to be L_h=5.03 cm, L_v=6.39 cm and U=0.4 cm/s. Figure 2 shows a top-down view at the vertical center of the vortex dipole numerically simulated, translating right to left for the purpose of the interactions of this work. The color bar represents vorticity magnitude; the vectors represent velocity. The mean velocity profile of the dipole as it translates left to right is the Gaussian profile shown in Figure 3.

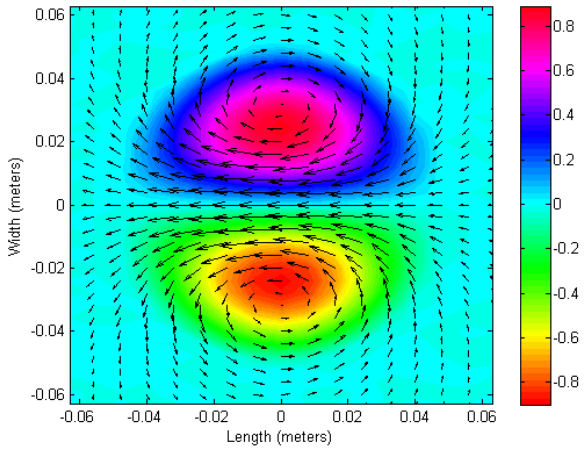

Figure 2: Lamb-Chaplygin vortex dipole numerically simulated. Vertical center, top-down view.

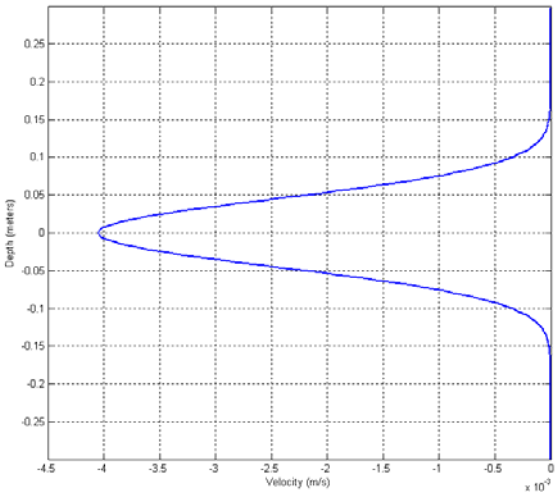

Figure 3: Vortex dipole's velocity profile with respect to depth (Gaussian in shape).

Results

Godoy-Diana, *et al.* (2006) reported bending of the wave beams during a co-propagating interaction. Figure 4 shows the evolution of this interaction for an initial relative frequency ω_r=0.2 s^{-1}. Figure 4a shows segments of three wave beams prior to the wave-vortex interaction. Figure 4b shows the middle wave beam of 4a bending to the horizontal as it interacts with the passing dipole. This is the internal waves of the beam propagating toward a critical level within the dipole. Figure 4c shows the same beam now absorbed by the dipole while the left-most beam is interacts with the front of the dipole. Figure 4d shows that the dipole has absorbed the energy of the wave beams. The dark spots along the beams are locations of defocusing of the off-center internal waves. This is to be discussed in more detail later.

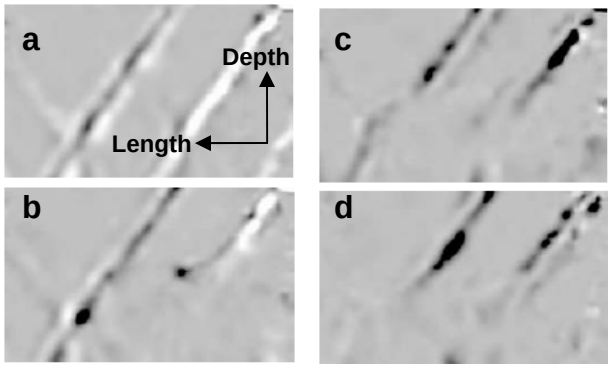

Figure 4: Two-dimensional view of experimental results from Godoy-Diana, *et al.* (2006) for the co-propagating case. Interactions shown are with the dipole jet as the dipole translates right to left. 4a shows the internal wave beams prior to the interaction. 4b shows one wave beam bending to the horizontal as the internal waves approach a critical level. 4c and d show the evolution of the interaction as the vortex absorbs the wave beams.

Figure 5 is the three-dimensional numerical simulation of this same interaction. Each line is a ray representing internal waves started at the same position along the length and the depth of the domain, but equally spaced along the width of the domain and above the vortices. Each ray was given the same initial wavenumber vector (k_1= -60 m^{-1}, k_2= 0 m^{-1}, k_3= 120 m^{-1}), for which k_3 was found using k_1, k_2 and ω_r with the dispersion relation (2). The length of the rays represents the wave propagation in time.

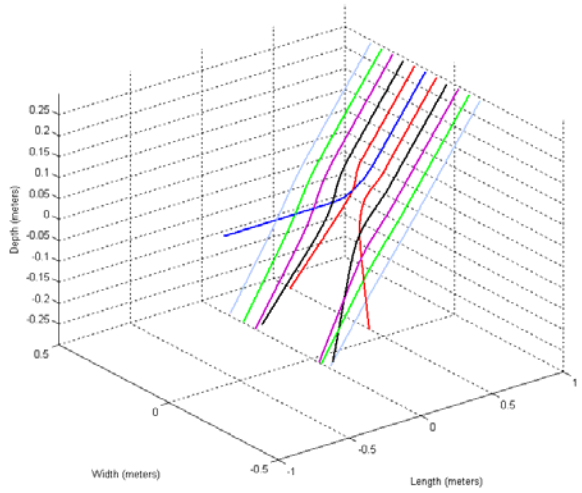

Figure 5: Three-dimensional view of co-propagating interaction using ray theory. Each line represents internal waves propagating in time through the space domain, having started at the same position along the length and depth and equally spaced along the width. Each ray began with the same initial wavenumber vector (k_1=-60 m^{-1}, k_2=0 m^{-1}, k_3=120 m^{-1}). The blue ray in center reached a critical level near z_C=5.6 cm above the depth center.

The center ray in blue reached a critical level near 5.6 cm above the center of the domain's depth as it interacted with the dipole jet. As the ray approached this depth, the relative frequency and the vertical group speed of the internal waves asymptotically approached zero. This is not unlike a two-dimensional internal wave interaction with a mean shear background having the profile of Figure (3). A zoomed-in view of the center ray's approach to the critical level is provided in Figure 6. The similarity to the bending of wave beams in Figure 4 validates the numerical simulation of the interaction. The approach to the critical level explains why the dipole of the experiment "erased" the wave beams, even below the dipole.

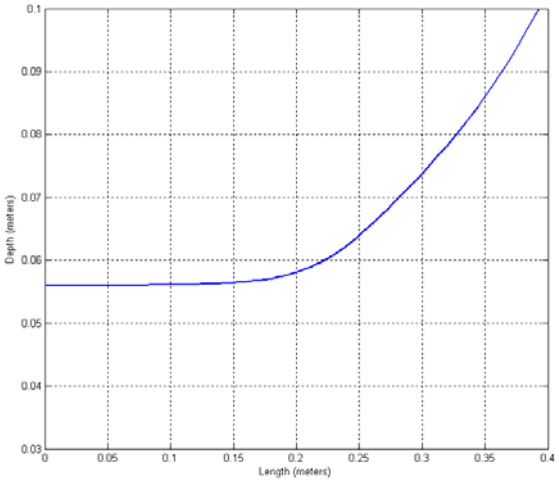

Figure 6: Center ray of Figure 5 approaching a critical level near z_C=5.6 cm above the center of the domain's depth.

Discussion

An important aspect of this numerical research includes the three-dimensional effects of the wave-vortex interaction. The defocusing of the co-propagating interaction is directly attributable to the three-dimensionality of internal wave propagation and the interaction with the vortex dipole. This discussion begins by considering Figure 4, the camera angle of which is spanwise to the domain. The two-dimensional view shows the evolution of the wave-vortex interaction at the center of the width of the domain, that is, along the jet of the dipole. The areas of darkness which show up along the beams during the interaction are locations of concentrated wave energy as the camera views it. They are, in fact, proof of defocusing, the term given by Godoy-Diana, *et al.* (2006) to describe the refraction and spanwise spreading of off-center rays. Figure 7 displays the defocusing, off-center internal waves in time (number of buoyancy periods) from a view above the interaction, with the dipole translating right to left. Locations where internal waves cross in time are likely areas of concentrated energy as seen by the camera.

Figure 8 shows the internal wave propagation in time during the interaction. It becomes obvious that the locations of internal waves crossing due to defocusing in Figure 7 do not correspond to any waves crossing in Figure 8. No waves were in the same position of width *and* length at the same time. This demonstrates clearly the need to consider three-dimensionality during such interactions.

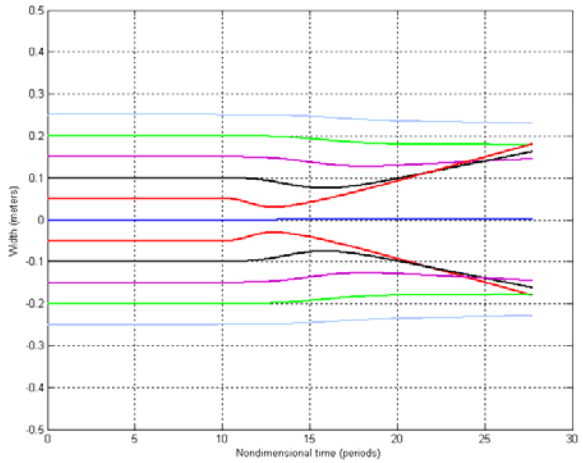

Figure 7: Top-down view of wave-vortex interaction, in buoyancy periods, given in Figure 5, with the vortex dipole translating right to left. The defocusing, or spanwise spreading, of the co-propagating internal waves is demonstrated. Concentrations of energy are expected to be where internal waves cross in time.

This is not, however, to say that the areas of energy concentration in Figure 4 are not that. While the numerical simulated interaction considered rays discretely and symmetrically placed about the center of the vortex dipole, the internal waves of the experiment were generated using a horizontal cylinder. The internal waves were continuously generated along the width of the domain. Thus, between the rays of the numerical simulation there may be locations where rays could have interacted with each other.

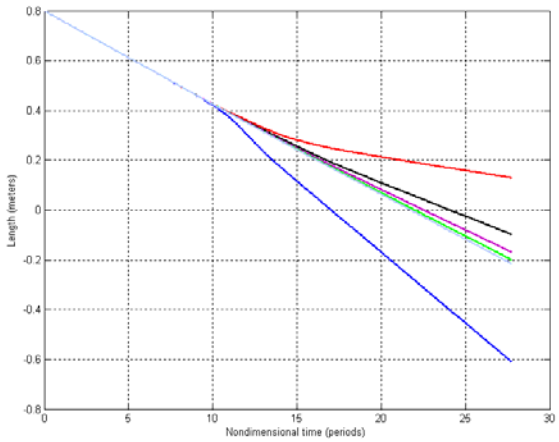

Figure 8: View of internal wave propagation in time. Crossed lines of internal waves in Figure 7 do not match to any crossings here. No internal waves interacted with each other.

Figure 9 shows the energy ratio (9) for the first interaction. The colored lines each correspond to the ray of the same color in Figure 5. The energetics of the interactions discussed is, thus far, surprising. If the vortex dipole was absorbing the energy of the center ray, the wave energy of the center ray would decrease as it approached the critical level because the relative frequency would have approached zero. This is not the case. Closer inspection of the wavenumbers (Figure 10) reveals that the wavenumber corresponding to domain length k_1 begins first to change, just after 8 buoyancy periods, but only slightly. The wavenumber corresponding to depth k_3 changes just after 9.5 buoyancy periods, but more dramatically, quickly increasing to infinity. Only then, at about 11.5 buoyancy periods, does the first horizontal wavenumber begin to increase rapidly in magnitude.

The sudden increase in magnitude of the wavenumbers distorts the dispersion relation, increasing the relative frequency and, in turn, the energy ratio (9) and Figure 9. A possible explanation follows, that nonlinear effects, such as wave overturning and breaking, may occur prior to any significant jump in wave energy or as a result of any sudden increase. This is feasible if the dipole yields its energy to the internal waves. More work is required to verify this possibility. Whether this is the case or not, research regarding this phenomenon is ongoing.

The numerical simulations of the counter-propagating interactions will follow the completed energy analysis of the co-propagating interaction. Needless to say, while the three-dimensionality of internal wave propagation and interaction poses special needs, it also greatly enhances physical understanding.

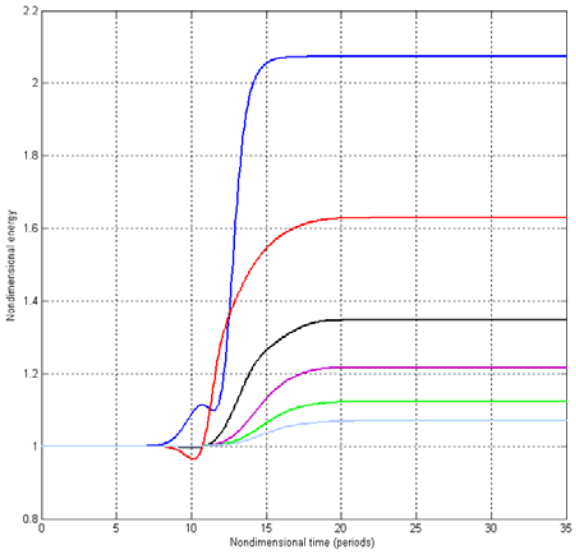

Figure 9: Energy ratio (9) for the interaction of Figures 5 and 8. Each colored line represents the energy ratio of the corresponding colored ray of these figures. The sudden energy increase is possibly related to nonlinearity in the interaction, untraceable by ray theory.

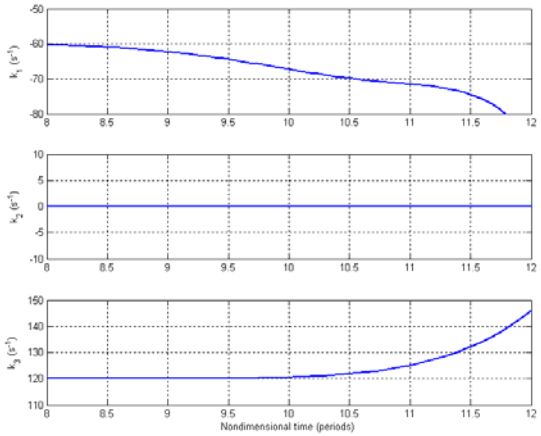

Figure 10: Wavenumbers of the center ray, as discussed for Figure 9.

References

Billant, P., Brancher, P. & Chomaz, J. (1999). Three-dimensional stability of a vortex pair. *Physics of Fluids*, *11*, 2069-2077.

Broutman, D. & Young, W.R. (1986). On the interaction of small-scale oceanic internal waves with near-inertial waves. *Journal of Fluid Mechanics*, *166*, 341-358.

Godoy-Diana, R., Chomaz, J. & Donnadieu, C. (2006). Internal gravity waves in a dipolar wind: A wave-vortex interaction experiment in a stratified fluid. *Journal of Fluid Mechanics*, *548*, 281-308.

Hayes, W.D. (1970). Kinematic Wave Theory. *Proceedings of the Royal Society of London. Series A, Mathematical and Physical Sciences, 320*, 209-226.

Javam, A., Imberger, J. & Armfield, S.W. (2000). Numerical study of internal wave-wave interactions in a stratified fluid. *Journal of Fluid Mechanics*, *415*, 65-87.

Moulin, F.Y. & Flór, J.-B. (2006). Vortex-wave interaction in a rotating stratified fluid: WKB simulations. *Journal of Fluid Mechanics*, *563*, 199-222.

Winters, Kraig B. & D'Asaro, Eric A. (1989). Two-Dimensional Instability of Finite Amplitude Internal Gravity Wave Packets Near a Crtical Level. *Journal of Geophysical Research*, *94*, 12,709-12,719.

Winters, Kraig B. & D'Asaro, Eric A. (1994). Three-dimensional wave instability near a critical level. *Journal of Fluid Mechanics*, *272*, 255-284.